

Forcing the Issue: Aromatic Tuning Facilitates Stimulus-Independent Modulation of a Two-Component Signaling Circuit

Morten H. H. Nørholm,[†] Gunnar von Heijne,[‡] and Roger R. Draheim^{*,§,||}

[†]Novo Nordisk Foundation Center for Biosustainability, Technical University of Denmark, Kogle Alle 6, DK-2970 Hørsholm, Denmark

[‡]Department of Biochemistry and Biophysics, Stockholm University, Svante Arrhenius väg 16C, SE-10691 Stockholm, Sweden

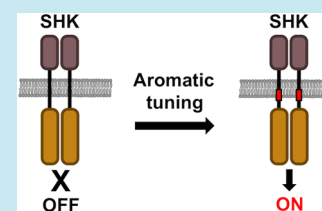
[§]Division of Pharmacy and ^{||}Wolfson Research Institute for Health and Wellbeing, Durham University, Queen's Campus, Stockton-on-Tees TS17 6BH, England, United Kingdom

Supporting Information

ABSTRACT: Two-component signaling circuits allow bacteria to detect and respond to external stimuli. Unfortunately, the input stimulus remains unidentified for the majority of these circuits. Therefore, development of a synthetic method for stimulus-independent modulation of these circuits is highly desirable because particular physiological or developmental processes could be controlled for biotechnological purposes without the need to identify the stimulus itself. Here, we demonstrate that aromatic tuning, i.e., repositioning the aromatic residues commonly found at the cytoplasmic end of the receptor (EnvZ) transmembrane domain, facilitates stimulus-independent modulation of signal output from

the EnvZ/OmpR osmosensing circuit of *Escherichia coli*. We found that these osmosensing circuits retained the ability to respond appropriately to increased external osmolarity, suggesting that the tuned receptors were not locked in a single conformation. We also noted that circuits containing aromatically tuned variants became more sensitive to changes in the receptor concentration than their wild-type counterpart, suggesting a new way to study mechanisms underpinning receptor concentration-dependent robustness. We believe that aromatic tuning has several advantages compared to previous methods aimed at stimulus-independent modulation of receptors and that it will be generally applicable to a wide-range of two-component circuits.

KEYWORDS: aromatic tuning, two-component circuit engineering, stimulus-independent modulation, concentration-dependent robustness



Two-component circuits are the most prevalent mechanism by which bacteria sense, respond, and adapt to external stimuli. These systems mediate responses to a wide range of environmental conditions such as nutrient availability, ambient temperature, or external osmolarity.¹ They also facilitate multiorganism phenomena such as quorum sensing, biofilm formation, and host–pathogen interaction.² In addition, they control essential environmental and agricultural processes such as chloroplast synthesis³ and root nodule formation.⁴ Therefore, development of a synthetic method for stimulus-independent modulation of these circuits is highly desirable because particular physiological or developmental processes could be controlled and characterized for biotechnological purposes without the need to identify the stimulus itself.

A canonical circuit consists of a membrane-spanning sensor histidine kinase (SHK) and a cytoplasmic response regulator (RR).¹ The largest group of SHKs possesses a periplasmic or extracellular domain responsible for stimulus perception. Subsequent signal transmission to the cell interior occurs via the adjacent transmembrane domain.⁵ Within the cytoplasm, most SHKs participate in both the phosphorylation (kinase activity) and dephosphorylation (phosphatase activity) of their cognate RR. For bifunctional SHKs, the extent of input stimulus controls the ratio of these activities, thereby governing the intracellular level of phosphorylated RR.⁶ Phosphorylation

of the RR modulates the activity of the covalently attached output domain, which usually interacts with DNA to control transcription of genes appropriate for mediating a response to the perceived stimulus.¹

A vast amount of genetic, biochemical, and structural information has been recently integrated into a “regulated unfolding” model of intraprotein signaling by modular proteins, including SHKs.⁷ This model proposes that modular proteins are composed of individual folding domains that contribute distinct functionalities. In the case of SHKs, it was suggested that the effector domain is maintained in an inactive conformation by a rigid connection between the stimulus perception and effector domains. Upon perception of stimulus, this structurally labile connection is disengaged, which, in turn, allows the effector domain to adopt an active conformation.⁷ Therefore, the regulated unfolding model suggests that the transmembrane (TM)–HAMP junction would be a suitable region to target with site-directed mutagenesis with the aim of destabilizing the coupling between the periplasmic stimulus-perceiving domain and any downstream signaling domains (Figure 1). Other results more explicitly support targeting this

Received: June 11, 2014

Published: August 27, 2014

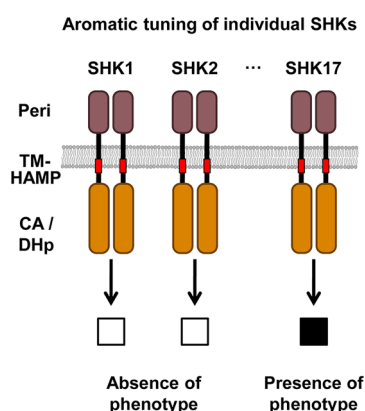


Figure 1. Synthetically tuning signal output from SHKs. In a canonical SHK, stimulus is perceived by the periplasmic domain (peri) and transmitted through the transmembrane (TM) and HAMP domains to the catalytic ATPase (CA) and dimerization/histidylphosphotransfer (DHp) domains. One potential example of employing aromatic tuning, i.e., repositioning the aromatic residues commonly found at the TM–HAMP junction, would be to assign downstream phenotypes to particular SHKs. Within an organism of interest, each SHK could be individually subjected to aromatic tuning (red boxes) and subsequently monitored for the phenotype of interest. If the appearance of the phenotype (filled box) correlated with aromatic tuning of a particular SHK, then this would suggest that the desired phenotype was governed by the aromatically tuned SHK.

region connecting TM to the HAMP domain, which is colloquially referred to as a “control cable”.^{8–15} We elected to focus on the aromatic residues found at the boundary of the control cable because they are conserved in many SHKs, which suggests that results generated here may be directly applicable to other membrane-spanning receptors.^{12,16}

To test the aromatic tuning approach within a well-characterized SHK, we have targeted the EnvZ/OmpR osmosensing circuit responsible for porin regulation within *Escherichia coli*. EnvZ is a canonical SHK that responds to changes in the extracellular osmolarity of inner-membrane impermeable compounds by modulating the intracellular level of phosphorylated OmpR (Figure 2A).^{17–20} Subsequently, phospho-OmpR regulates the transcription of a number of

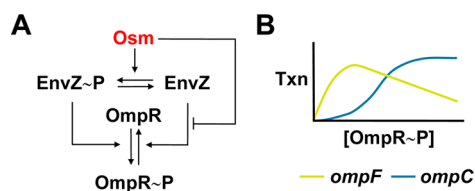


Figure 2. The EnvZ/OmpR osmosensing circuit of *E. coli* was subjected to aromatic tuning. The phosphorylated and unphosphorylated forms of EnvZ and OmpR are in equilibrium. EnvZ is a bifunctional SHK that phosphorylates and dephosphorylates its cognate RR, OmpR. Osmotic pressure (Osm), due to the presence of small inner-membrane-impermeable solutes, alters the ratio of these activities resulting in a net increase of intracellular OmpR-P. In this study, osmotic pressure (red) was induced by growing cells in the presence of sucrose. (B) The intracellular level of OmpR-P governs transcription (Txn) of *ompF* (yellow) and *ompC* (blue). Here, transcription was monitored by employing strain MDG147 that contains a transcriptional fusion of *yfp* to *ompF* and of *cfp* to *ompC*. This allows intracellular levels of OmpR-P to be estimated by calculating the CFP/YFP ratio.

genes, including those encoding two outer membrane porins, OmpF and OmpC. At low intracellular levels of phospho-OmpR (OmpR-P), transcription of *ompF* is upregulated, whereas at higher levels of OmpR-P, transcription of *ompF* is repressed and transcription of *ompC* is activated. This results in a predominance of OmpF at low osmolarity and OmpC at higher osmolarity (Figure 2B).^{21–23} The easily controllable nature of the input stimulus and the well-characterized transcriptional output makes the EnvZ/OmpR osmosensing circuit an ideal choice for examining aromatic tuning within an SHK.

Aromatic tuning of EnvZ demonstrated that repositioning the Trp-178/Lue-179/Phe-180 triplet located at the TM–HAMP junction was sufficient to modulate signal output. We found that these tuned osmosensing circuits retained the ability to respond appropriately to additional external osmolarity, which demonstrates that the tuned EnvZ receptors possess altered steady-state signal output but were not locked in a single conformation. We also noted that osmosensing circuits containing aromatically tuned receptors became more sensitive to changes in EnvZ levels than their wild-type counterpart, pointing to a new way of studying the mechanisms underpinning receptor concentration-dependent robustness within two-component circuits. We conclude by discussing the general applicability of aromatic tuning to a wide-range of two-component circuits and the advantages of this strategy compared to those previously aimed at stimulus-independent modulation of signal output. This is highly desirable because particular biological processes could be controlled in the absence of stimulus identification.

RESULTS AND DISCUSSION

Measurement of Steady-State Signal Output from the EnvZ/OmpR Osmosensing Circuit. To analyze steady-state signal output from EnvZ/OmpR osmosensing circuits containing aromatically tuned receptors, the two-color fluorescent reporter strain MDG147²⁴ was used. MDG147 is a derivative of strain K-12 MG1655 that possesses transcriptional fusions of *cfp* to *ompC* and of *yfp* to *ompF* within its chromosome (Figure 2B). Quantifying the ratio of CFP to YFP fluorescence provides a rapid and sensitive measure of the ratio of *ompC* to *ompF* transcription, which estimates the intracellular level of phosphorylated OmpR. MDG147 cells harboring the control vector pEB5²⁵ were grown in glucose minimal medium containing increasing amounts of sucrose to increase signal output from the EnvZ/OmpR osmosensing circuit. As previously reported, MDG147 cells exhibited an increase in *ompC* transcription, as indicated by increased CFP fluorescence, and a decrease in *ompF* transcription, shown by decreased YFP fluorescence (Figure S1A).²⁴ These results confirm that the ratio of CFP to YFP fluorescence (CFP/YFP) can be used to estimate the intracellular phospho-OmpR levels (Figure S1B).

Strain EPB30²⁶ is an *envZ*[−] derivative of MDG147 that is suitable to assess the effects of plasmid-based *envZ* expression. EPB30 cells were complemented with plasmid pEnvZ²⁷ or pRD400, a derivative expressing a V5-epitope tagged version of EnvZ. pRD400 maintains the IPTG-based induction of pEnvZ while adding a previously used heptaresidue linker of Gly-Gly-Ser-Ser-Ala-Ala-Gly and the V5 epitope tag to the C-terminus of EnvZ.^{12–15,28–30} The wild-type and epitope-tagged versions of EnvZ were induced by addition of a wide range of IPTG concentrations, and the steady-state signal output of the various

osmosensing circuits was analyzed. Comparisons of CFP fluorescence, YFP fluorescence, or the CFP/YFP ratio of plasmid-complemented EPB30 cells grown under the low (0% sucrose) or high (15% sucrose) osmolarity regimes demonstrated that an intermediate range of IPTG concentrations was required to maintain steady-state signal output when either wild-type or the epitope-tagged version of EnvZ was present (Figure S2). Under either the low and high osmolarity regimes, steady-state signal output, as defined by CFP/YFP in EPB30/pRD400 cells, was similar to that of MDG147/pEB5 cells when EnvZ-V5 was induced by addition of between roughly 10 and 50 μ M IPTG (Figure S2).

Immunoblotting against the V5 epitope was performed to gain a quantitative understanding of the composition of osmosensing circuits containing EnvZ-V5 (Figure S3). When grown under either the low or high osmolarity regimes, osmosensing circuits within EPB30/pRD400 cells could tolerate a roughly 10-fold range in EnvZ-V5 levels while retaining steady-state signal output similar to MDG147/pEB5 cells (Figure 3). It is important to note that EnvZ-V5 levels outside this range resulted in changes of CFP fluorescence but not YFP fluorescence, as previously reported (Figure S4).²⁵

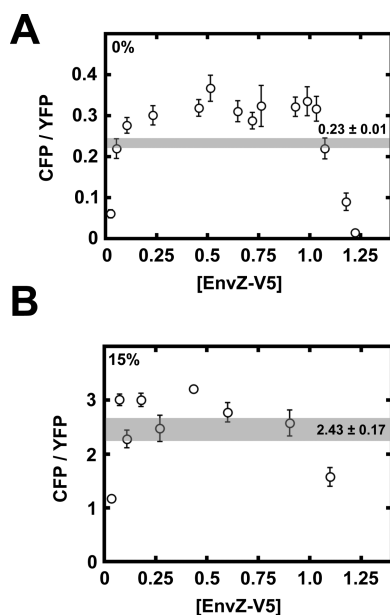


Figure 3. Steady-state signal output from osmosensing circuits possessing increasing amounts of EnvZ-V5. Under the low (A) or high (B) osmolarity regimes, osmosensing circuits in EPB30/pRD400 (open circles) cells possess steady-state signal output similar to that of MDG147/pEB5 over a broad range of receptor levels. The receptor level was determined by comparison to a control band within each lane on an immunoblot (see Figure S3). Error bars represent standard deviation of the mean with a sample size of $n \geq 3$. The transparently shaded area represents the mean of the steady-state signal output within MDG147/pEB5 cells with a range of one standard deviation of the mean ($n \geq 3$).

Aromatic Tuning Modulates Steady-State Signal Output from the EnvZ/OmpR Circuit. To determine whether the steady-state signal output from osmosensing circuits was altered upon aromatic tuning, we created a series of EnvZ-V5 receptors in which the Trp-178/Leu-179/Phe-180 triplet was repositioned (Figure 4). This series of receptors was expressed over a large range of IPTG concentrations, and

```

169
170
171
172
173
174
175
176
177
178
179
180
181
182
183
184
185
186
EnvZ WLF-5: IMLLWLEAIGGAIQNR
EnvZ WLF-4: IMLLAWLEFIGGAIQNR
EnvZ WLF-3: IMLLATWLEGGAIQNR
EnvZ WLF-2: IMLLAIGWLEFGAIQNR
EnvZ WLF-1: IMLLAIGGWLEFAIQNR
EnvZ WLF 0: IMLLAIGGAWLEFRIQNR
EnvZ WLF+1: IMLLAIGGAGWLEFRIQNR
EnvZ WLF+2: IMLLAIGGAGGWLEFIQNR

```

Figure 4. Primary sequence of the C-terminal end of TM2 from the aromatically tuned EnvZ variants. A Trp-Leu-Phe triplet was repositioned, and the minus series of receptors has the triplet repositioned in the N-terminal direction while the plus series of receptors has the Trp-Leu-Phe triplet repositioned in the C-terminal direction. EnvZ WLF 0 is the wild-type receptor. Residue positions within EnvZ are provided above the primary sequences.

immunoblotting techniques similar to those described in Figure S3 were used to estimate the extent of receptor expression.

During our analysis, we assessed whether osmosensing circuits containing the aromatically tuned variants possessed normal levels of CFP fluorescence, YFP fluorescence, and CFP/YFP ratios. We also assessed whether these values were constant regardless of the amount of tuned EnvZ-V5 present. When EPB30 (*envZ*⁻) cells are grown under the low or high osmolarity regime and express untuned or aromatically tuned EnvZ-V5 from pRD400, the CFP/YFP ratio can be used to estimate the intracellular level of phosphorylated OmpR (Figure S1).²⁵

In the uppermost panels of Figure 5, we illustrate that osmosensing circuits tolerate a broad range of EnvZ-V5 levels (same data as that in Figures 3 and S4). When EPB30/pRD400 cells were grown under the low osmolarity regime, steady-state CFP fluorescence was attained between EnvZ-V5 levels of 0.1 and 1.0. Likewise, when these cells were grown under the high osmolarity regime, steady-state CFP fluorescence was maintained between EnvZ-V5 levels of 0.1 and 0.9. In contrast, steady-state YFP fluorescence was observed over the entire range of EnvZ-V5 levels examined. CFP/YFP ratios were dependent on attaining steady-state CFP fluorescence, so the range of EnvZ-V5 required for reaching steady-state was the same as that for CFP fluorescence alone. Trendlines are provided over the ranges of EnvZ-V5 levels where normal signal output was attained. These trendlines were subsequently replicated within the other panels to aid in comparison.

We began by comparing CFP/YFP ratios from circuits containing an aromatically tuned variant to the circuit containing the untuned EnvZ-V5 (left panels in Figure 5). It is noteworthy that circuits containing the aromatically tuned variants of EnvZ-V5 did not show the expected decrease in CFP/YFP at higher levels of EnvZ-V5; therefore, all data points above EnvZ-V5 levels of 0.1 were included during calculation of subsequent trendlines. Under the low osmolarity regime, circuits containing the minus series of receptors (WLF-5 through WLF-1) achieved steady-state output at least equal to that of circuits containing the untuned receptor, as indicated by a CFP/YFP ratio of approximately 0.30–0.35 (compare the light green and light gray trendlines in the left panels of Figure 5). However, within certain circuits, such levels of signal output were attained only at higher EnvZ-V5 levels. This can be observed as the light green trendline passing through the light gray trendline. Circuits containing the plus-series of receptors (WLF+1 and WLF+2) failed to attain normal signal output. In

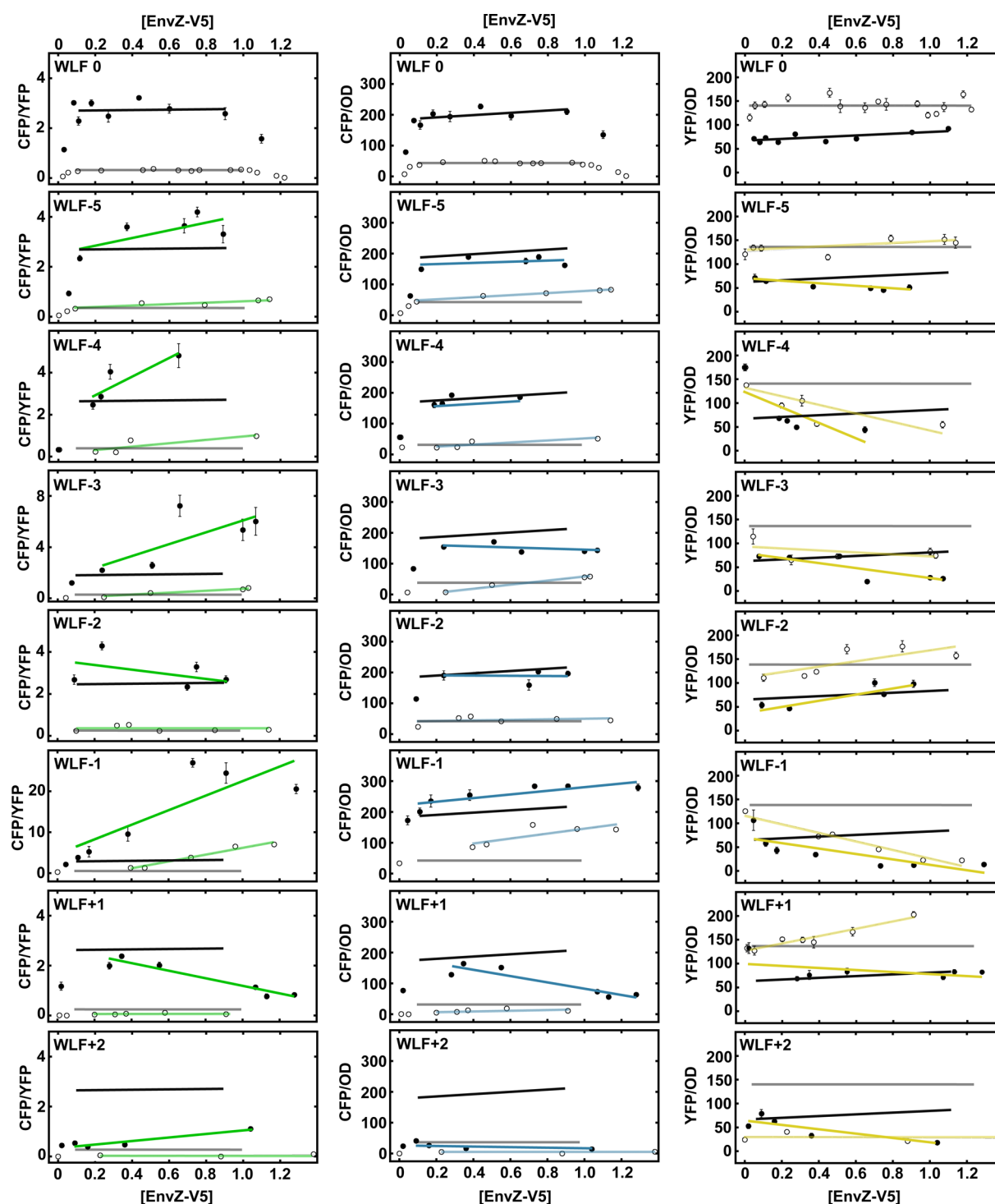


Figure 5. Steady-state signal output from osmosensing circuits containing the WLF series of tuned EnvZ receptors. CFP/YFP ratio (left panels), CFP fluorescence (center panels), or YFP fluorescence (right panels) are presented for osmosensing circuits containing one of the aromatically tuned receptors. The amount of receptor present is determined as described in Figure S3. Osmosensing circuits containing the untuned receptor are presented at the top of the figure (WLF 0). Data from EPB30/pRD400 cells grown under the low (open circles) and high (filled circles) osmolarity regimes are shown. These trendlines are present in all charts for comparison to the results from circuits containing the aromatically tuned variants. Trendlines for cells grown under the low osmolarity regime are presented as light gray lines, while those from cells grown under the high osmolarity regime are shown as dark lines. CFP fluorescence was steady between EnvZ-V5 levels of 0.1 and 1.0 when cells were grown under the low osmolarity regime and between EnvZ-V5 levels of 0.1 and 0.9 when grown under the high osmolarity regime. This is in contrast to YFP, which remains steady over the entire range of EnvZ-V5 levels. CFP/YFP was affected by the reduction of CFP fluorescence at either end of the spectrum. However, no reduction in CFP or CFP/YFP was observed at higher levels of the tuned EnvZ-V5 variants. Thus, when determining the trendlines for CFP fluorescence or CFP/YFP for circuits containing the tuned variants, only EnvZ-V5 levels above 0.1 were considered. For circuits containing the tuned variants, the light and dark green lines represent CFP/YFP ratios for EPB30/pRD400 cells grown under the low and high osmolarity regimes, respectively. Likewise, CFP and YFP fluorescence are represented as light and dark blue and yellow trendlines, respectively.

these cases, the light green trendline never passes through the light gray trendline. When EPB30/pRD400 cells were grown under the high osmolarity regime, we observed similar results. All circuits, with the exception of those containing the WLF+1 or WLF+2 variant, possessed a CFP/YFP that equals or exceeds signal output from those containing the untuned variant (i.e., a CFP/YFP ratio of ~ 2.5 – 3.0). Again, this was usually observed at higher receptor levels (compare solid green and black trendlines in the left panels of Figure 5). The steady-state output of several circuits exhibited large changes in CFP/YFP ratio that were dependent on EnvZ-V5 level. To facilitate a more quantitative comparison between circuits, we have calculated the slope (m) of each trendline (Table S1). Of the circuits that attained normal steady state-signal output, changes based on EnvZ-V5 level were notable for those containing the WLF-4 ($m = +4.5$), WLF-3 ($m = +4.5$), and WLF-1 ($m = +18$) variants and to a lesser extent for circuits containing the WLF-5 ($m = +1.5$) variant.

To gain a further understanding of steady-state signal output from these circuits, we compared changes in the extent of CFP or YFP fluorescence individually (center and right panels of Figure 5, respectively). When cells were grown under the low osmolarity regime, the absolute CFP fluorescence for circuits containing all of the minus series of receptors (WLF-5 through WLF-1) achieved steady-state signal output greater than that from circuits containing untuned EnvZ-V5, and again, this usually occurred at higher receptor levels (compare light cyan and gray trendlines in the center panels). Cells containing circuits with WLF+1 and WLF+2 did not attain normal steady-state CFP fluorescence, even at higher receptor levels. When cells were grown under the high osmolarity regime, only circuits containing the WLF+1 or WLF+2 variants did not approach normal steady-state levels of CFP (compare solid cyan and black trendlines in the center panels). We also observed that circuits containing several tuned variants appeared to be sensitive to the level of EnvZ-V5 present under the low osmolarity regime. This included circuits containing the WLF-5 ($m = +35$), WLF-4 ($m = +32$), WLF-3 ($m = +62$), and WLF-1 ($m = +78$) variants. Under the high osmolarity regime, the WLF-5 through WLF-2 variants resulted in levels of CFP fluorescence similar to that of circuits containing the untuned variant. Circuits containing WLF-1 remained elevated compared to that of the untuned variant. Interestingly, the WLF+1 variant resulted in a slight decrease in CFP fluorescence at high expression levels, and, in a similar manner to the low osmolarity regime, the WLF+2 variant never resulted in normal levels of CFP fluorescence.

When grown under the low osmolarity regime, circuits containing the WLF-5 variant were the only circuits that approximated YFP fluorescence from circuits containing the untuned receptor (compare the light yellow and gray trendlines in the right panels). Those containing the WLF-4 ($m = -90$), WLF-3 ($m = -18$), and WLF-1 ($m = -91$) variants exhibited a sharp decrease in YFP fluorescence as increasing levels of the tuned variant were present. This is in contrast to circuits containing the WLF-2 ($m = +60$) and WLF+1 ($m = +77$) variants, which produced slightly greater than normal YFP fluorescence as the receptor levels increased, while circuits containing WLF+2 never attained normal YFP fluorescence. The observed trends were similar when cells were grown under the high osmolarity regime, with the exception of circuits containing WLF+1 not exhibiting greater than normal levels of

YFP fluorescence (compare solid yellow and black trendlines in the right panels).

Correlation between the Surface of TM2 the Aromatic Residues Reside upon and Signal Output. One manner in which to compare these trends is to plot them along the abscissa of the schematic in Figure 2B in order to estimate the intracellular level of phospho-OmpR. However, analyzing the data in this manner does pose an issue as the absolute CFP and YFP levels supported by some variants change based on their level of expression. In essence, the further the slope (m) in Table S1 is away from 0, the less tolerance a circuit possesses for changes in EnvZ-V5 level. Therefore, we have selected receptor concentrations of 0.2, 0.5, and 0.8 based on the results from circuits containing untuned variants. In Figure 6, we plot

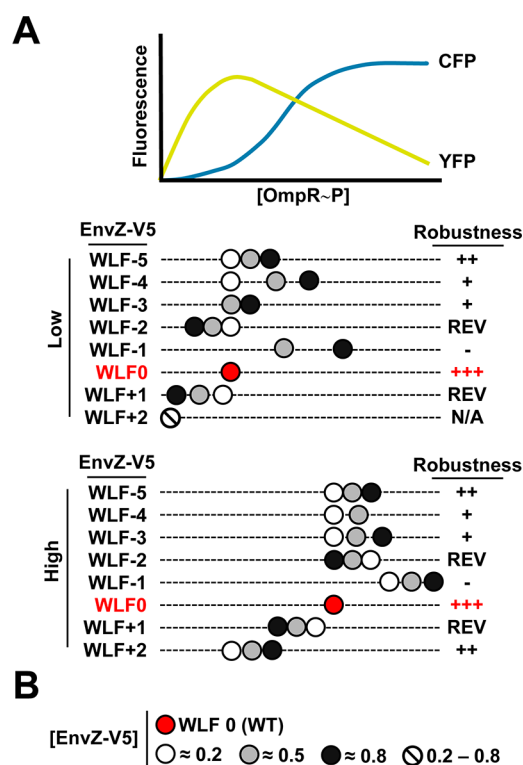


Figure 6. Comparison of signal output from osmosensing circuits containing the various aromatically tuned EnvZ receptors. Steady-state signal output from circuits containing the WLF series of aromatically tuned variants expressed in EPB30/pRD400 cells grown under the low (upper panel) or high (lower panel) osmolarity regime is shown. The intracellular levels of phospho-OmpR are estimated through use of the antisymmetrical reporter system presented in Figure 2B. Signal output at low (open circles), medium (gray circles), and high levels (filled circles) of EnvZ-V5 expression (0.2, 0.5, and 0.8, respectively) is presented for comparison. The extent of sensitivity to changes in the amount of EnvZ present is also summarized as robustness. In this column, N/A represents not applicable, as in there is no reasonable amount of signal output, whereas REV indicates reversed, where a decrease in activity is observed as the level of EnvZ-V5 increases. This evaluation of robustness correlates with the slope (m) in Table S1.

data for cells grown under the low and high osmolarity regimes. By plotting the data in this manner, we are able to estimate the steady-state intracellular level of phospho-OmpR while taking into account three parameters: the effect of aromatic tuning, any concentration-dependent effects (i.e., robustness), and the role of osmolarity on modulating EnvZ signal output.

Under the low osmolarity regime, most circuits containing little tuned EnvZ-V5, i.e., an [EnvZ-V5] of 0.2, possessed signal output similar to that of wild-type circuits. The exception is those containing the WLF+2 variant, which exhibits essentially no CFP or YFP fluorescence regardless of the amount of receptor present. Circuits containing the WLF-2 and WLF+1 variants exhibited decreasing signaling output as the amount of receptor present is increased, which manifested as increasing YFP fluorescence ($m = +62.57$ and $+20.42$, respectively). The other tuned variants, e.g., WLF-5, WLF-4, WLF-3, and WLF-1, all result in increased signal output as the amount of receptor present is increased, i.e., a slope of CFP/YFP trendline > 0 . In most cases, this was observed as increased levels of CFP fluorescence ($m > 0$) and decreased levels of YFP fluorescence ($m < 0$), with the WLF-1 variant exemplifying this phenotype (Table S1). Under the high osmolarity regime, a similar pattern is observed, except that the mutants are shifted toward the right end of the curve, as expected (Figure 6).

In summary, the majority of osmosensing circuits containing aromatically tuned receptors resulted in increased in signal output as EnvZ-V5 levels increased, with the exception of those containing the WLF-2 or WLF+1 variants, which resulted in decreased signal output. Circuits containing the WLF+2 variants always possessed the lowest signal output.

These results suggest that aromatic tuning is sufficient to modulate EnvZ signal output in a manner that correlates with the surface of TM2 that the residues are placed upon. One interpretation of this data would be to suggest that the movement of the aromatic residues destabilizes the TM–HAMP junction in manner that mimics signal output; however, additional experimentation would be required to confirm this hypothesis (Figure S5). Although the aromatic residues were repositioned, other residues substitutions occurred, which may also contribute to changes in signal output. One possible example would be the loss of the Arg-182 from the WLF+2 variant. We did not explicitly examine the change in the charge density, but we do address it indirectly below.

To ensure that aromatic tuning was not restricted to these particular residues (Trp-Leu-Phe), another series of aromatically tuned EnvZ receptors was created. However, this time a Trp-Tyr-Ala triplet was employed at the same initial residue positions of 178–180 (Figure S6). In this case, the Trp and Tyr residues were selected because they were previously moved within the aspartate chemoreceptor of *E. coli* (Tar).^{12,13} However, in order to keep the changes as similar as possible between these sets of aromatically tuned receptors, i.e., moving a triplet, an alanyl residue was also repositioned (Trp-Tyr-Ala). We employed the same techniques (Figure S7), and the data is consistent with the TM2 surface being critical (Figure S8), but additional experimentation is required to demonstrate whether this is due to steric repulsion between individual helices at the cytoplasmic end of the TM domain. In addition, the data from the WYA+2 variant demonstrates that Arg-182 is not essential for EnvZ function, suggesting that maintenance of charge density in this region is not critical.

Advantages of Employing Aromatic Tuning To Modulate SHK Signal Output. We believe that employing aromatic tuning to facilitate stimulus-independent modulation should be applicable to other SHKs because previously published alignments of primary sequences demonstrate that the majority of SHKs in *E. coli* possess aromatic residues at the cytoplasmic polar/hydrophobic interface.^{12,16} In addition, the majority of aromatically tuned EnvZ variants retain the ability

to respond to stimulus (Figures 6 and S8), suggesting that their signal output is biased but not locked in either a stimulus-deprived or -saturated conformation. In this regard, aromatic tuning is advantageous compared to deletion of entire SHKs³¹ or substitution of the conserved His residue involved in autophosphorylation and phosphotransfer because such methods may result in complete loss of kinase or phosphatase activity. Complete loss of activity has been shown to result in nonphysiological cross-talk between various two-component signaling pathways within a cell.^{32,33} On the basis of our results, we propose that aromatic tuning could be used to rapidly assign downstream physiological and developmental processes to particular SHKs (Figure 1).

Using Aromatic Tuning To Study Receptor Concentration-Dependent Robustness. Increased sensitivity to changes in SHK levels was seen for all osmosensing circuits containing an aromatically tuned EnvZ variant. A previous kinetic model predicted that the steady-state output of the EnvZ/OmpR osmosensing circuit should be insensitive to fluctuations in the concentration of EnvZ.²⁵ A related model that predicts a stronger form of robustness with respect to the regulatory proteins was also recently analyzed.³⁴ In both cases, the steady-state signal output of the signaling circuit should be independent of the level of SHK, which was observed when wild-type EnvZ or EnvZ-V5 was present within the circuit (Figures 3 and S2–S4). This robustness was observed previously within the intact EnvZ/OmpR,²⁵ PhoQ/PhoP,³⁵ and CpxA/CpxR²⁶ circuits. Here, for each aromatically tuned variant, a different relationship between steady-state signal output and receptor level was observed, apparent as a change in the slope of the CFP/YFP trendlines that are summarized in Table S1, suggesting that the ratio of kinase to phosphatase activities was different within each receptor and always different than wild-type EnvZ (Figures 5 and S6). Therefore, we propose that further biochemical examination of this series of aromatically tuned receptors will provide insight into the precise mechanisms underpinning receptor concentration-dependent robustness within two-component signaling circuits.

METHODS

Bacterial Strains and Plasmids. *E. coli* strain MC1061 [F^- *araD139* Δ (*ara-leu*)7696 Δ (*lac*)X74 *galU galK hsdR2*(r_K^- m_K^-) *mcrB1 rpsL*]³⁶ was used for all DNA manipulations. Strain MG1655 (F^- λ^- *ilvG rfb50 rph1*) was used to control for light scattering and cellular autofluorescence. Strains MDG147 [MG1655 Φ (*ompF*⁺-*yfp*⁺) Φ (*ompC*⁺-*cfp*⁺)]²⁴ and EPB30 (MDG147 *envZ::kan*)²⁶ were used for analysis of the steady-state signal output from osmosensing circuits.

To analyze steady-state signal output from osmosensing circuits, plasmid pRD400 was made by adding an in-frame coding sequence for a seven-residue linker (GGSSAAG)²⁹ and a C-terminal V5 epitope tag (GKPIPPLLGLDST).³⁷ PCR amplification was employed to create a product with a 5'-terminus containing a BglII site corresponding to the internal site within *envZ* and a 3'-terminus encoding the linker, epitope tag, and a SalI restriction site. This product was subsequently cloned into pEnvZ²⁷ with BglII and SalI, resulting in the removal of an approximately 800 bp region between the previous stop codon in *envZ* and the SalI site. This strategy was used to retain similar IPTG-based induction of EnvZ and EnvZ-V5 from pEnvZ and pRD400, respectively. A previously described plasmid, pEB5,²⁵ served as an empty vector control that did not express *envZ*.

Analysis of Steady-State Signal Output from Osmensing Circuits. Analysis was performed as described previously²⁵ with slight modification. Briefly, MDG147²⁴ or EPB30²⁶ cells were transformed with pEBS,²⁵ pEnvZ,²⁷ or pRD400 as required. Fresh colonies were used to inoculate 2 mL overnight cultures of minimal medium A³⁸ supplemented with 0.2% glucose. Ampicillin, sucrose, and IPTG were added where appropriate. Cells were grown overnight at 37 °C and diluted at least 1:1000 into 7 mL of fresh medium. Chloramphenicol was added to a final concentration of 170 µg/mL to inhibit protein synthesis when the cultures reached an OD_{600nm} ~ 0.3. Fluorescent analysis was immediately conducted with 2 mL of culture, while the remainder was centrifuged and stored at -80 °C for immunoblotting. All fluorescence measurements were performed with a Varian Cary Eclipse (Palo Alto, CA). CFP fluorescence was measured by using an excitation wavelength of 434 nm and an emission wavelength of 477 nm, while YFP fluorescence was measured by using an excitation wavelength of 505 nm and an emission wavelength of 527 nm. These values were corrected for differences in cell density by dividing the fluorescent intensities by OD_{600 nm} and for light scattering and cellular autofluorescence by subtracting the CFP and YFP fluorescence intensities determined for MG1655/pEBS cells.

Protein Quantification of EnvZ-V5. Pellets from cells expressing EnvZ-V5 were analyzed on 12% SDS/acrylamide gels. Standard buffers and conditions were used for electrophoresis and immunoblotting.³⁹ Anti-V5 (Invitrogen) and anti-β-lactamase (Abcam) primary antibodies were used. Peroxidase-conjugated anti-mouse IgG (Sigma) was used as the secondary antibody. Bands were visualized with the ECL advance western blotting detection kit (GE Healthcare). Digitized images were acquired with a Lumi-Imager F1 workstation (Roche) and analyzed with Image Gauge v4.22 software (Fujifilm). Intensities of the β-lactamase bands served as an internal control for cell density and sample loading.

■ ASSOCIATED CONTENT

● Supporting Information

Various control experiments described throughout the text (Figures S1–S4). A model proposing how the aromatic residues influence signal output (Figure S5). Data for the WYA (Trp-Tyr-Ala) series of aromatically tuned variants (Figures S6–S8). The slopes of the trendlines from Figures 5 and S7 (Table S1). This material is available free of charge via the Internet at <http://pubs.acs.org>.

■ AUTHOR INFORMATION

Corresponding Author

*Tel.: +44 191 334 0694. Fax: +44 191 334 0374. E-mail: roger.draheim@durham.ac.uk

Notes

The authors declare no competing financial interest.

■ ACKNOWLEDGMENTS

Members of the von Heijne group and Martin Kurnik (Aarhus University) provided valuable support and discussion during the early stages of this project. We thank Mark Goulian (University of Pennsylvania) for several strains that were used during this experimentation. R.R.D. was supported by a Kirschstein National Research Service Award from the National Institutes of Health (AI075573) during the initial stages of this

project. This work was also supported by a grant from the Lundbeck Foundation to M.H.H.N. and by grants from the Swedish Foundation for Strategic Research, the Swedish Research Council, and the Swedish Cancer Foundation to G.v.H.

■ REFERENCES

- (1) Stock, A. M., Robinson, V. L., and Goudreau, P. N. (2000) Two-component signal transduction. *Annu. Rev. Biochem.* 69, 183–215.
- (2) Novick, R. P., and Geisinger, E. (2008) Quorum sensing in staphylococci. *Annu. Rev. Genet.* 42, 541–564.
- (3) Puthiyaveetil, S., Kavanagh, T. A., Cain, P., Sullivan, J. A., Newell, C. A., Gray, J. C., Robinson, C., van der Giezen, M., Rogers, M. B., and Allen, J. F. (2008) The ancestral symbiont sensor kinase CSK links photosynthesis with gene expression in chloroplasts. *Proc. Natl. Acad. Sci. U.S.A.* 105, 10061–10066.
- (4) David, M., Daveran, M. L., Batut, J., Dedieu, A., Domergue, O., Ghai, J., Hertig, C., Boistard, P., and Kahn, D. (1988) Cascade regulation of nif gene expression in *Rhizobium meliloti*. *Cell* 54, 671–683.
- (5) Mascher, T., Helmann, J. D., and Uden, G. (2006) Stimulus perception in bacterial signal-transducing histidine kinases. *Microbiol. Mol. Biol. Rev.* 70, 910–938.
- (6) Russo, F. D., and Silhavy, T. J. (1993) The essential tension: opposed reactions in bacterial two-component regulatory systems. *Trends Microbiol.* 1, 306–310.
- (7) Schultz, J. E., and Natarajan, J. (2013) Regulated unfolding: a basic principle of intraprotein signaling in modular proteins. *Trends Biochem. Sci.* 38, 538–545.
- (8) Parkinson, J. S. (2010) Signaling mechanisms of HAMP domains in chemoreceptors and sensor kinases. *Annu. Rev. Microbiol.* 64, 101–122.
- (9) Park, H., Im, W., and Seok, C. (2011) Transmembrane signaling of chemotaxis receptor tar: insights from molecular dynamics simulation studies. *Biophys. J.* 100, 2955–2963.
- (10) Zhou, Q., Ames, P., and Parkinson, J. S. (2009) Mutational analyses of HAMP helices suggest a dynamic bundle model of input–output signalling in chemoreceptors. *Mol. Microbiol.* 73, 801–814.
- (11) Kitanovic, S., Ames, P., and Parkinson, J. S. (2011) Mutational analysis of the control cable that mediates transmembrane signaling in the *Escherichia coli* serine chemoreceptor. *J. Bacteriol.* 193, 5062–5072.
- (12) Draheim, R. R., Bormans, A. F., Lai, R. Z., and Manson, M. D. (2005) Tryptophan residues flanking the second transmembrane helix (TM2) set the signaling state of the Tar chemoreceptor. *Biochemistry* 44, 1268–1277.
- (13) Draheim, R. R., Bormans, A. F., Lai, R. Z., and Manson, M. D. (2006) Tuning a bacterial chemoreceptor with protein–membrane interactions. *Biochemistry* 45, 14655–14664.
- (14) Wright, G. A., Crowder, R. L., Draheim, R. R., and Manson, M. D. (2011) Mutational analysis of the transmembrane helix 2-HAMP domain connection in the *Escherichia coli* aspartate chemoreceptor tar. *J. Bacteriol.* 193, 82–90.
- (15) Adase, C. A., Draheim, R. R., Rueda, G., Desai, R., and Manson, M. D. (2013) Residues at the cytoplasmic end of transmembrane helix 2 determine the signal output of the TarEc chemoreceptor. *Biochemistry* 52, 2729–2738.
- (16) Boldog, T., and Hazelbauer, G. L. (2004) Accessibility of introduced cysteines in chemoreceptor transmembrane helices reveals boundaries interior to bracketing charged residues. *Protein Sci.* 13, 1466–1475.
- (17) Egger, L. A., Park, H., and Inouye, M. (1997) Signal transduction via the histidyl–aspartyl phosphorelay. *Genes Cells* 2, 167–184.
- (18) Forst, S. A., and Roberts, D. L. (1994) Signal transduction by the EnvZ–OmpR phosphotransfer system in bacteria. *Res. Microbiol.* 145, 363–373.

(19) (1995) *Two-Component Signal Transduction* (Hoch, J. A., and Silhavy, T. J., Eds.) ASM Press, Washington, DC.

(20) Mizuno, T. (1998) His–Asp phosphotransfer signal transduction. *J. Biochem.* 123, 555–563.

(21) Forst, S., Delgado, J., Rampersaud, A., and Inouye, M. (1990) *In vivo* phosphorylation of OmpR, the transcription activator of the ompF and ompC genes in *Escherichia coli*. *J. Bacteriol.* 172, 3473–3477.

(22) Lan, C. Y., and Igo, M. M. (1998) Differential expression of the OmpF and OmpC porin proteins in *Escherichia coli* K-12 depends upon the level of active OmpR. *J. Bacteriol.* 180, 171–174.

(23) Russo, F. D., and Silhavy, T. J. (1991) EnvZ controls the concentration of phosphorylated OmpR to mediate osmoregulation of the porin genes. *J. Mol. Biol.* 222, 567–580.

(24) Batchelor, E., Silhavy, T. J., and Goulian, M. (2004) Continuous control in bacterial regulatory circuits. *J. Bacteriol.* 186, 7618–7625.

(25) Batchelor, E., and Goulian, M. (2003) Robustness and the cycle of phosphorylation and dephosphorylation in a two-component regulatory system. *Proc. Natl. Acad. Sci. U.S.A.* 100, 691–696.

(26) Siryaporn, A., and Goulian, M. (2008) Cross-talk suppression between the CpxA–CpxR and EnvZ–OmpR two-component systems in *E. coli*. *Mol. Microbiol.* 70, 494–506.

(27) Hsing, W., and Silhavy, T. J. (1997) Function of conserved histidine-243 in phosphatase activity of EnvZ, the sensor for porin osmoregulation in *Escherichia coli*. *J. Bacteriol.* 179, 3729–3735.

(28) Adase, C. A., Draheim, R. R., and Manson, M. D. (2012) The residue composition of the aromatic anchor of the second transmembrane helix determines the signaling properties of the aspartate/maltose chemoreceptor Tar of *Escherichia coli*. *Biochemistry* 51, 1925–1932.

(29) Cantwell, B. J., Draheim, R. R., Weart, R. B., Nguyen, C., Stewart, R. C., and Manson, M. D. (2003) CheZ phosphatase localizes to chemoreceptor patches via CheA-short. *J. Bacteriol.* 185, 2354–2361.

(30) Wright, G. A., Crowder, R. L., Draheim, R. R., and Manson, M. D. (2010) Mutational analysis of the TM2-HAMP connection in TarE, the *E. coli* aspartate receptor. *J. Bacteriol.* 193, 82–90.

(31) Zhou, L., Lei, X. H., Bochner, B. R., and Wanner, B. L. (2003) Phenotype microarray analysis of *Escherichia coli* K-12 mutants with deletions of all two-component systems. *J. Bacteriol.* 185, 4956–4972.

(32) Groban, E. S., Clarke, E. J., Salis, H. M., Miller, S. M., and Voigt, C. A. (2009) Kinetic buffering of cross talk between bacterial two-component sensors. *J. Mol. Biol.* 390, 380–393.

(33) Siryaporn, A., and Goulian, M. (2010) Characterizing cross-talk *in vivo* avoiding pitfalls and overinterpretation. *Methods Enzymol.* 471, 1–16.

(34) Shinar, G., Milo, R., Martinez, M. R., and Alon, U. (2007) Input output robustness in simple bacterial signaling systems. *Proc. Natl. Acad. Sci. U.S.A.* 104, 19931–19935.

(35) Miyashiro, T., and Goulian, M. (2008) High stimulus unmasks positive feedback in an autoregulated bacterial signaling circuit. *Proc. Natl. Acad. Sci. U.S.A.* 105, 17457–17462.

(36) Casadaban, M. J., and Cohen, S. N. (1980) Analysis of gene control signals by DNA fusion and cloning in *Escherichia coli*. *J. Mol. Biol.* 138, 179–207.

(37) Southern, J. A., Young, D. F., Heaney, F., Baumgartner, W. K., and Randall, R. E. (1991) Identification of an epitope on the P and V proteins of simian virus 5 that distinguishes between two isolates with different biological characteristics. *J. Gen. Virol.* 72, 1551–1557.

(38) Miller, J. H. (1992) *A Short Course in Bacterial Genetics: A Laboratory Manual and Handbook for Escherichia coli and Related Bacteria*, Cold Spring Harbor Laboratory Press, Plainview, NY.

(39) Ausubel, F. M., Brent, R., Kingston, R. E., Moore, D. D., Seidman, J. G., Smith, J. A., and Struhl, K. (1998) *Current Protocols in Molecular Biology*, Wiley, New York.